This is an open access article published under a Creative Commons Non-Commercial No Derivative Works (CC-BY-NC-ND) Attribution License, which permits copying and redistribution of the article, and creation of adaptations, all for non-commercial purposes.

CHEMISTRY OF MATERIALS
Cite This: Chem. Mater. 2019, 31, 5075−5080
Article
pubs.acs.org/cm

Black Phosphorus/Palladium Nanohybrid: Unraveling the Nature of P−Pd Interaction and Application in Selective Hydrogenation

Matteo Vanni,[†,○] Manuel Serrano-Ruiz,[†] Francesca Telesio,[‡] Stefan Heun,[‡] Martina Banchelli,[§] Paolo Matteini,[§] Antonio Massimiliano Mio,[∥] Giuseppe Nicotra,[∥] Corrado Spinella,[∥] Stefano Caporali,[⊥] Andrea Giaccherini,[#] Francesco D'Acapito,[▽] Maria Caporali,*[,†] and Maurizio Peruzzini*[,†]

[†]CNR-ICCOM, Via Madonna del Piano10, 50019 Sesto Fiorentino, Italy
[‡]NEST Istituto Nanoscienze—CNR and Scuola Normale Superiore, Piazza S. Silvestro 12, 56127 Pisa, Italy
[§]CNR-IFAC, Via Madonna del Piano10, 50019 Sesto Fiorentino, Italy
[∥]CNR-IMM Istituto per la Microelettronica e Microsistemi, VIII strada 5, I-95121 Catania, Italy
[⊥]Department of Industrial Engineering, University of Florence, Via di S. Marta 3, 50139 Florence, 50139, Italy
[#]Department of Earth Sciences, University of Florence, Via La Pira 4, 50121 Firenze, Italy
[▽]CNR-IOM-OGG, c/o European Synchrotron Radiation Facility, 71 Avenue des Martyrs, CS 40220, 38043 Grenoble, Cedex 9 France
[○]Department of Biotechnology, Chemistry and Pharmacy, University of Siena, 53100 Siena, Italy

Supporting Information

ABSTRACT: The burgeoning interest in two-dimensional (2D) black phosphorus (bP) contributes to the expansion of its applications in numerous fields. In the present study, 2D bP is used as a support for homogeneously dispersed palladium nanoparticles directly grown on it by a wet chemical process. Electron energy loss spectroscopy−scanning transmission electron microscopy analysis evidences a strong interaction between palladium and P atoms of the bP nanosheets. A quantitative evaluation of this interaction comes from the X-ray absorption spectroscopy measurements that show a very short Pd−P distance of 2.26 Å, proving for the first time the existence of an unprecedented Pd−P coordination bond of a covalent nature. Additionally, the average Pd−P coordination number of about 1.7 reveals that bP acts as a polydentate phosphine ligand toward the surface of the Pd atoms of the nanoparticles, thus preventing their agglomeration and inferring with structural stability. These unique properties result in a superior performance in the catalytic hydrogenation of chloronitroarenes to chloroanilines, where a higher chemoselectivity in comparison to other heterogeneous catalyst based on palladium has been observed.

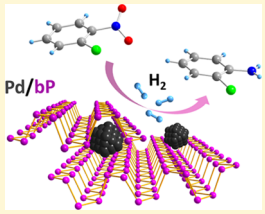

INTRODUCTION

With the advent of molybdenum disulfide and black phosphorus (bP) as two-dimensional (2D) materials, which have attracted the common interests of physicists, chemists, and material scientists, the postgraphene era has just started. The peculiar physical properties of bP are incidently between those of graphene and transition-metal dichalcogenides, such as the direct tunable energy band gap (0.3 eV in the bulk, 1.8 eV for the monolayer) and the high carrier mobility at room temperature (1000 $cm^2/(V\ s)$), which are desirable for high-performance mechanically flexible field-effect transistor devices.[1] bP has a unique puckered honeycomb structure derived from the sp^3 hybridization of phosphorus atoms, which, in turn, gives rise to a strong in-plane anisotropy of many physical properties, such as heat and electron flow, which vary in the armchair and zigzag direction, respectively.[2] Furthermore, the presence of a lone pair on each P-atom opens the way to several surface modifications. Indeed, several studies have addressed the chemical functionalization of bP, either covalent[3,4] or not,[5,6] with the aim to improve the processability of the material and the ambient stability,[2−7] which is the Achille's heel of bP. A growing field is the study of bP as a support for metal and metal phosphide nanoparticles (NPs) to trigger applications in catalysis. Taking advantage of its intrinsic property of being a semiconductor, few-layer bP has been tested in the photocatalytic processes, either alone or in combination with a metal as a co-catalyst, in hydrogen evolution reaction,[8] water-splitting,[9] and photodegradation of organic pollutants.[10,11] Other catalytic applications as hydrogenation and oxidation of organic compounds have been shown for various M NPs/bP nanohybrids, where M = Au,[12] Co,[13] Ni,[14] Pt,[15] and recently Pd NPs have been anchored on anatase TiO_2−bP hybrid for ethanol electro-oxidation.[16] Nevertheless, up to now, there is no experimental study focusing on the nature of the chemical interaction between metal nanoparticles and P atoms of bP. Our current work represents an important step in this direction since we found out that a strong covalent bond does exist between Pd NPs and

Received: March 1, 2019
Revised: June 21, 2019
Published: July 3, 2019

Downloaded via UNIV DEGLI STUDI DI FIRENZE on November 6, 2019 at 14:11:51 (UTC).
See https://pubs.acs.org/sharingguidelines for options on how to legitimately share published articles.

© 2019 American Chemical Society

DOI: 10.1021/acs.chemmater.9b00851
Chem. Mater. 2019, 31, 5075−5080

bP. This interaction is responsible for the high stability of this material and contributes in explaining its remarkable performance in the catalysis.

EXPERIMENTAL SECTION

Materials. All manipulations were performed under inert atmosphere using Schlenk techniques. $Pd(NO_3)_2{\cdot}2H_2O$, 1-chloro-2-nitrobenzene, and 1-chloro-3-nitrobenzene were used as received from Sigma-Aldrich. Ketjen black EC 600JD (surface area = 1400 m^2/g) was purchased from Akzo Nobel. Black phosphorus (bP) was prepared according to the literature procedure[17] and the liquid-phase exfoliation of bP was performed according to a protocol set up in our laboratories.[18]

Synthesis of the Nanohybrid Pd/bP. Exfoliated black phosphorus was suspended in degassed tetrahydrofuran to have a concentration of 1.0 mg/mL. This suspension (1.5 mL; 1.5 mg of bP, 0.048 mmol) was transferred to a glass vial equipped with a stirring bar and put inside a Schlenk tube. Under stirring, 0.75 mL of degassed ethanol was added, followed by 1.3 mL of an aqueous solution of $Pd(NO_3)_2{\cdot}\ 2H_2O$ (3.75 mM, 4.87 μmol, molar ratio P/Pd = 10). The vial was transferred in an autoclave, pressurized with 5 bar of H_2 and kept on a stirring plate at room temperature for 1 h. After this time, the autoclave was vented, the catalyst Pd/bP settled down at the bottom of the vial, and the colorless supernatant was removed by a syringe. Five milliliters of degassed ethanol was added, and Pd/bP was resuspended by sonication and transferred to a centrifugation tube. After centrifugation at 9000 RPM for 30 min, the supernatant was discarded, and the washing procedure was repeated two times. The solid material was then collected and dried under vacuum for 10 h. The actual composition of the nanohybrid was evaluated with an inductively coupled plasma atomic emission spectrometer measuring both Pd and P. The resulting Pd content was 10.6 mol %. The yield of this preparation, as determined from the final P content, was 88% due to minor material losses during the work-up procedure. The nanohybrid Pd/bP with 0.5 mol % loading of Pd used for comparison in Raman characterization was prepared following the same procedure.

RESULTS AND DISCUSSION

First, the synthesis of crystalline black phosphorus was carried out according to the procedure developed by Nilges et al.,[17] wherein high-purity red phosphorus, tin, and a catalytic amount of SnI_4 are heated at 650 °C in a muffle oven for 3 days. Afterward, bP nanosheets were obtained by liquid-phase exfoliation of bP microcrystals suspended in dimethylsulfoxide and kept under the action of ultrasound for several hours.[18] Palladium nanoparticles were grown on the surface of the bP nanosheets using dihydrate $Pd(NO_3)_2$ as a precursor and hydrogen gas as a reducing agent, see Experimental Section. The morphology of the new 2D material, Pd/bP, was first studied by scanning electron microscopy (SEM), which shows that Pd NPs are embedded in the bP nanosheets, see Figure 1a. Inspection by transmission electron microscopy (TEM), high-angle annular dark-field scanning transmission electron microscopy (HAADF STEM), and energy-dispersive X-ray spectroscopy (EDS) confirmed the formation of nearly spherical palladium nanoparticles homogeneously distributed on the bP nanosheets and with a relative narrow size distribution centered at 3.1 ± 0.8 nm, see Figure 1b–d. Atomic force microscopy (AFM) revealed the presence of both thin and thick flakes with a mean size of around 600 nm and a thickness increasing from 5 to 200 nm (Figures 1e and S4).

The nanohybrid Pd/bP was characterized by powder X-ray diffraction (XRD), which confirms the phase purity of the 2D material and shows a strong preferential orientation along the (0k0) direction, with three most intense peaks at 2θ = 16.8, 34.2, and 52.2° assigned to the (020), (040), and (060) planes of orthorhombic black phosphorus, respectively (Figure 2a).

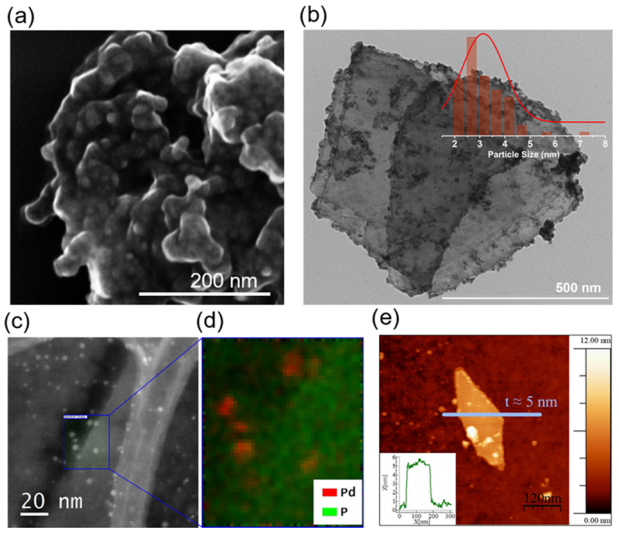

Figure 1. Structural characterization of Pd/bP. (a) SEM image of Pd/bP. (b) Transmission electron microscopy (TEM) image of Pd/bP and relative size distribution. Scale bar: 500 nm. (c) High-resolution HAADF STEM image of Pd/bP on a lacey carbon grid. Pd-rich areas can be clearly distinguished for the higher Z-contrast (brighter areas). The blue region of interest indicates the region in which the EDS SI (spectrum imaging) was performed. (d) EDS elemental mapping of the selected area on Pd/bP obtained by integrating the signals from the Pd L-lines and the P K-lines. (e) AFM image of a Pd/bP flake on Si/SiO_2. The line corresponds to the cross-sectional profile shown as an inset. The flake thickness is approximately 5 nm.

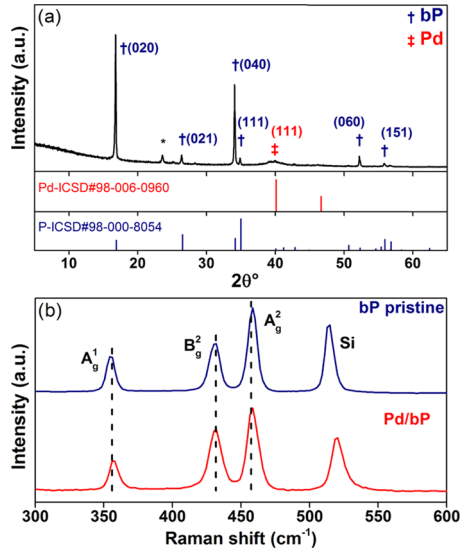

Figure 2. (a) XRD spectrum of Pd/bP. (b) Comparison of Raman spectra collected on the pristine bP (red) and Pd/bP (blue). Each spectrum has been obtained combining the data from 15 different flakes.

This is also a characteristic of the pristine material, suggesting that its crystalline structure is retained upon functionalization with Pd NPs. A very broad peak at around 2θ = 39.5°, which is assigned to the (111) planes of Pd, confirms the presence of a nanosized fcc phase of the metal.

DOI: 10.1021/acs.chemmater.9b00851
Chem. Mater. 2019, 31, 5075–5080

It is well established[19] that the three Raman peaks of bP at 357.8, 431.5, and 459.2 cm^{-1} corresponding to the Raman active phonon modes of A_g^1, B_g^2, and A_g^2, respectively, depend on the thickness and may undergo a frequency shift with varying flake thickness. Given the thickness the polydispersity of bP prepared by sonochemical exfoliation, micro-Raman spectra were collected for a large set of flakes to take into account the broad range of thickness. As shown in Figure 2b, the Raman spectrum of Pd/bP displays three peaks, characteristic of the orthorombic phase of bP observed above by XRD; however, no significant frequency shift was detected compared to the pristine bP. Figure S5 shows a detailed statistics for A_g^1, B_g^2, and A_g^2 Raman modes of the pristine bP and Pd/bP.

Electron energy loss spectroscopy (EELS) is an important tool to gain information on the chemical shifts in the core-level states, as well as on the fine structure of the unoccupied valence-band states; thus, we performed a comparative EELS analysis between bP (simulated[20] and measured) and Pd/bP measured by HAADF-STEM-SI (see Figure 3). A difference in the P L-edge is observed in the energy range 138−140 eV for Pd/bP, which reveals a modification of the electronic structure of bP, which can be interpreted as the result of an interaction between the P atoms of bP and Pd NPs.

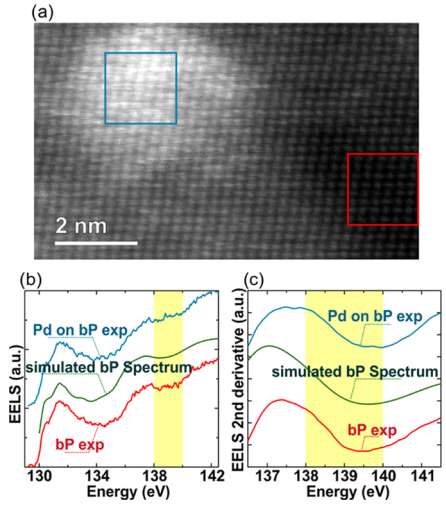

Figure 3. (a) HAADF-STEM-SI of Pd/bP acquired along the [101] zone axis at the P L-edge. (b) EELS spectra: red curve, experimental bP, obtained by integrating the EELS-SI (spectrum imaging) along the red box in (a); green curve: simulated bP;[20] blue curve: experimental Pd/bP, obtained by integrating the EELS-SI along the blue box in (a). (c) Second derivative plots of the three EELS spectra within the region highlighted in (b).

The chemical states of the Pd NPs were determined by the Pd 3d core-level X-ray photoelectron spectroscopy (XPS) spectrum (Figure 4a), which is fitted by the use of two doublets due to spin−orbit couplings. The components at binding energy (B.E.) = 335.8 eV (Pd $3d_{5/2}$) and at B.E. = 341.0 eV (Pd $3d_{3/2}$) accounts for bulk metallic palladium.[21] The smaller doublet at B.E. = 338.1 and 343.5 eV is attributable to an electrodepleted palladium species, probably with an oxidation state of +2. The presence of PdO can be ruled out because the peaks with corresponding B.E. values are absent;[22] thus, the signal at higher binding energy can be explained as the result of a partial valence orbital overlap between surface Pd atoms and bP nanosheets. The presence of a layer of electron-depleted palladium atoms on the surface of

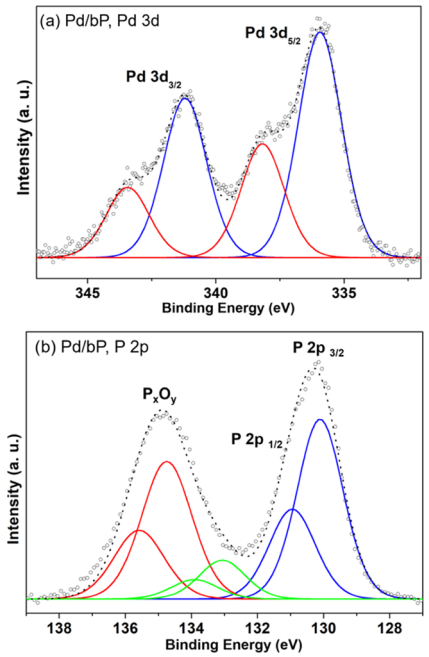

Figure 4. (a) Pd 3d core-level XPS spectrum of Pd/bP. Metallic and electron-depleted palladium doublets are depicted by blue and red lines, respectively. (b) P 2p core-level XPS spectrum of Pd/bP.

Pd NPs, which strongly interacts with P atoms, has been already observed[23] in the study of Pd NPs capped with the phosphine ligand PTA (PTA = 1,3,5-triaza-7-phophaadamantane), which indeed shows a comparable XPS spectrum.

The deconvolution of the P 2p core-level spectrum of the pristine bP shows the characteristic doublet representing the P $2p_{3/2}$ and P $2p_{1/2}$ peaks located at 129.7 and 130.6 eV, typical for elemental phosphorus (see Figure S7). Interestingly, the P 2p core-level spectrum of Pd/bP is much more complex, requiring the use of at least three components. Besides the doublet attributable to elemental phosphorus (two peaks at B.E. = 130 and 131 eV), components at higher B.E. values are also present (see Figure 4b), which can be interpreted as due to phosphorus in different chemical environments. The doublet at intermediate B.E. values (green line fitting in Figure 4b) is likely due to the P−Pd bonds. The large doublet characterized by the highest binding energy (red line fitting in Figure 4b) accounts for the presence of phosphorus oxides species such as P−OH, P═O, and P−O−P on the surface of the bP sheets.[24] Since peaks at lower B.E. values characteristic of P having a phosphide nature (128.6 eV)[25] are absent, the presence of phosphides as Pd_xP_y can be excluded.

To the best of our knowledge, the nature of the interaction between metal nanoparticles and bP has been so far approached only by theoretical calculations. For instance, the nanohybrid Ag/bP has been described as stabilized by covalent bonds at the Ag/bP interface by means of density functional theory (DFT) calculations,[10] but no experimental investigations have been carried out till date. To unravel the nature of the Pd−P interaction, X-ray absorption spectroscopy measurements were performed on Pd/bP, and the following compounds were taken as standards: PdO, Pd NPs capped with the phosphine ligand PTA and labeled as Pd@PTA,[23] palladium phosphide nanoparticles PdP_2 NPs,[26] Pd NPs supported on carbon Pd/C,[27] and Pd metal foil (see Table S1).

DOI: 10.1021/acs.chemmater.9b00851
Chem. Mater. 2019, 31, 5075−5080

The raw extended X-ray absorption fine structure (EXAFS) spectra and the corresponding Fourier transforms are shown in Figure 5. The peak just below 2 Å in the sample Pd/bP is at

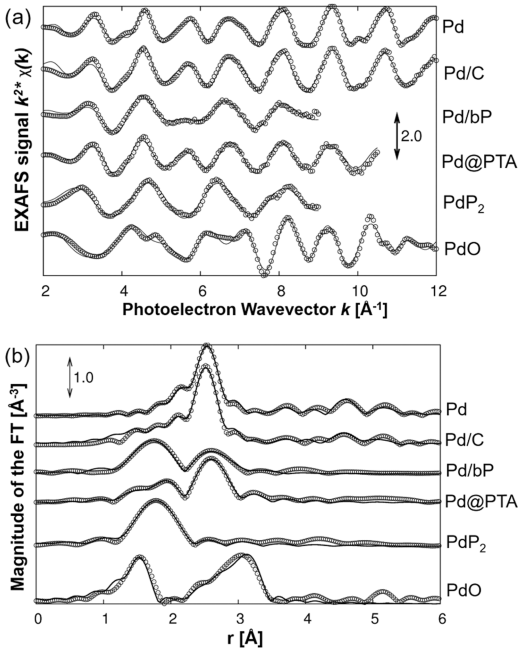

Figure 5. (a) EXAFS data at the Pd K-edge, and (b) the corresponding Fourier transforms. Dots are experimental data, while continuous lines are the calculated best-fit data.

higher r value if compared with the PdO peak, thus suggesting the presence of a ligand different from oxygen in Pd/bP. A comparison with the FTs shows a position for this peak very close to the PdP_2 feature and the quantitative data could be fitted only using the P ligands for Pd. Attempts with O have led to unphysical results, which is obvious because O and P atoms have substantially different backscattering functions and appreciably different bond length values (R_{PdO} = 2.00 Å, R_{PdP} = 2.26 Å, see the Supporting Information (SI)). Thus, the peak below 2 Å in the sample Pd/bP can be safely assigned to the Pd−P bonds. A second peak just below 3 Å can be inferred to the Pd−Pd bonds, being present in Pd metal foil, Pd/C, and Pd@PTA. This means that Pd atoms are involved in two different bonds: Pd−Pd and Pd−P; the former arises from the bonds with the inner metal atoms of the nanoparticle, while the latter arises from the interaction between the surface Pd atoms and P atoms of bP. The accurate values of the bond length were obtained from these data by fittings and are shown in Table S2. Noteworthy, the short Pd−P distance, R_{PdP} = 2.26(3) Å, found in Pd/bP points out that the latter is a very strong interaction. As a comparison, the phosphide PdP_2 has longer bonds, R_{PdP} = 2.32(2) Å, according to our measurement and are in agreement with literature.[28] PdP_3 has[29] R_{PdP} = 2.235 Å, which is close to that of Pd/bP, see Table S2, but the presence of phosphide can be surely excluded in our sample on the basis of the XPS measurements previously discussed. Remarkably, Pd@PTA exhibits R_{PdP} = 2.25 Å, which is consistent with the coordination bond distance Pd−P of 2.203(3) Å measured[30] in the X-ray structure of the complex cation $[Pd(PTAH)_4]^{4+}$, and it is almost the same value measured for Pd/bP. This reveals the Pd−P interaction in Pd/bP can be seen as a coordination bond of covalent nature and closely resembles the one existing in Pd@PTA: the P atoms of the bP nanosheets surround Pd NPs acting similar to the molecular phosphine ligand PTA toward Pd NPs. This folding agrees well with the morphology observed by SEM, see Figure 1a, and also explains the stacking of the flakes observed by AFM, see Figure S4. The observed average Pd−P coordination number CNs = 1.7(6) in our sample, see the SI, fairly corroborates this picture.

This detailed structural study demonstrates that bP nanosheets may act as polydentate phosphorus ligand toward metal nanoparticles via coordination bonds. This strong interaction confers a stabilization to Pd NPs, preventing their agglomeration, and makes Pd/bP a good candidate for catalysis. Intrigued by these results, the reduction of chloronitroarenes to the corresponding chloroanilines was selected as the model reaction (see Scheme 1). The latter are

Scheme 1. Hydrogenation of Chloronitroarenes to Chloroanilines

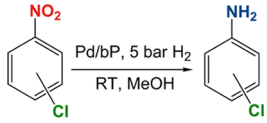

highly valuable intermediates for the manufacture of many agrochemicals, pharmaceuticals, polymers, and dyes.[31] Since traditional methods employing stoichiometric reducing agents have drawbacks due to both economic and environmental issues, efforts have been devoted to replace them with hydrogen gas. However, many tested catalysts are severely affected by undesired dehalogenation due to the C−Cl hydrogenolysis (see Figure S8), thus finding a catalyst able to efficiently carry out a chemoselective reduction of nitroarenes remains a challenge.

Satisfyingly, Pd/bP showed a very high chemoselectivity in the reduction of both *ortho*- and *meta*-chloronitrobenzenes, showing 97.3% selectivity toward chloroaniline at 99.5% conversion for the ortho isomer (see Table S3), surpassing other heterogeneous catalysts based on Pd NPs[32] that are affected by dehalogenation. As a comparison, bare Pd NPs with similar average sizes were grown on a highly porous carbon, ketjen black, see the SI; at complete conversion, the chemoselectivity dropped down to 78.1%, the remaining being 21.9% pure aniline, as shown in Table S3. This means that in the presence of Pd/C, the secondary reaction of C−Cl hydrogenolysis takes place simultaneously with NO_2 reduction, while with Pd/bP, first NO_2 is reduced to NH_2 and then C−Cl hydrogenolysis starts. In the case of hydrophobic charcoal, affinities to both chloronitrobenzene and chloroaniline are expected to be comparable and once chloroaniline is formed, presumably its desorption from the surface is slow, and this leads to hydrogenolysis. On the other hand, the adsorption of NO_2 molecule on the surface of bP is known to be a highly favored process from energy point of view.[33] Therefore, we expect the nitroarene to be easily adsorbed on Pd/bP; however, once the nitro group is hydrogenated to amine, the latter is desorbed from the surface of Pd/bP, impeding the secondary reaction of C−Cl hydrogenolysis to take place. DFT calculations are in progress to elucidate the mechanism under action and to validate this model.

Catalyst reuse was also tested, showing the selectivity was maintained unaltered for six consecutive runs; only a small

DOI: 10.1021/acs.chemmater.9b00851
Chem. Mater. 2019, 31, 5075−5080

decrease of the conversion was observed (see Figure S9). In agreement with this, TEM investigation on Pd/bP recovered after the catalytic runs, confirmed that the morphology was preserved, with the average size of Pd NPs being 3.6 ± 0.9 nm (see Figure S10). The heterogeneous nature of our catalyst was proved as well with an independent test (see Table S4). Thus, the presence of Pd−P bonds prevents the bP degradation and provides excellent structural stability to our catalyst.

CONCLUSIONS

In summary, a new Pd/bP nanohybrid has been developed and the nature of the interaction between Pd NPs and bP nanosheets elucidated by EXAFS. A very short Pd−P distance of 2.26(3) Å was disclosed, accounting for a coordinative bond of covalent nature between the surface Pd atoms and P atoms. Moreover, the average Pd−P coordination number turned out to be 1.7(6), which suggests that bP acts as a polydentate phosphine ligand toward Pd NPs, stabilizing them toward agglomeration and preventing the leaching of the metal in solution. Pd NPs are thus embedded between bP flakes to yield a new 0D−2D heterostructure. Finally, the synergy between Pd NPs and bP was successfully exploited in the reduction of chloronitroarenes to the corresponding chloroanilines, showing a far superior chemoselectivity in comparison to other heterogeneous catalysts based on palladium. Furthermore, Pd/bP was reused and maintained its efficiency after six consecutive runs, demonstrating an intrinsic stability that promises further applications in various fields.

ASSOCIATED CONTENT

Supporting Information

The Supporting Information is available free of charge on the ACS Publications website at DOI: 10.1021/acs.chemmater.9b00851.

Experimental methods, including synthesis of the nanohybrid Pd/ketjen black, instruments and characterization, supporting figures, tables, discussion, and references; additional TEM, HAADF-STEM, XRD, AFM, Raman, and EELS; tables contain EXAFS data and catalytic tests (PDF)

AUTHOR INFORMATION

Corresponding Authors

*E-mail: maria.caporali@iccom.cnr.it (M.C.).
*E-mail: maurizio.peruzzini@iccom.cnr.it (M.P.).

ORCID

Francesca Telesio: 0000-0003-3834-3685
Stefan Heun: 0000-0003-1989-5679
Andrea Giaccherini: 0000-0003-0915-1318
Maria Caporali: 0000-0001-6994-7313

Notes

The authors declare no competing financial interest.

ACKNOWLEDGMENTS

Thanks are expressed to EC for funding the project PHOSFUN "Phosphorene functionalization: a new platform for advanced multifunctional materials" (ERC ADVANCED GRANT to M.P.). STEM-EELS analysis was performed at Beyond-Nano CNR-IMM, which is supported by the Italian Ministry of Education and Research (MIUR) under project Beyond-Nano (PON a3_00363). The authors gratefully acknowledge for SEM and TEM images "Ce.M.E.—Centro Microscopie Elettroniche Laura Bonzi" in Sesto Fiorentino (Italy) financed by "Ente Cassa di Risparmio di Firenze" and through the projects "EnergyLab", POR FESR 2014-2020, and FELIX (Fotonica ed Elettronica Integrate per l'Industria, project code no. 6455). Finally, MIUR is kindly acknowledged for financial support through Project PRIN 2015 (grant number 20154X9ATP).

REFERENCES

(1) Li, L.; Yu, Y.; Ye, G.; Ge, Q.; Ou, X.; Wu, H.; Feng, D.; Chen, X. H.; Zhang, Y. Black Phosphorus Field-Effect Transistors. *Nat. Nanotechnol.* **2014**, *9*, 372−377.

(2) Gusmão, R.; Sofer, Z.; Pumera, M. Black Phosphorus Rediscovered: from Bulk Material to Monolayers. *Angew. Chem., Int. Ed.* **2017**, *56*, 8052−8072.

(3) Sofer, Z.; Luxa, J.; Bouša, D.; Sedmidubský, D.; Lazar, P.; Hartman, T.; Hardtdegen, H.; Pumera, M. The Covalent Functionalization of Layered Black Phosphorus by Nucleophilic Reagents. *Angew. Chem., Int. Ed.* **2017**, *56*, 9891−9896.

(4) van Druenen, M.; Davitt, F.; Collins, T.; Glynn, C.; O'Dwyer, C.; Holmes, J. D.; Collins, G. Covalent Functionalization of Few-Layer Black Phosphorus using Iodonium Salts and Comparison to Diazonium Modified Black Phosphorus. *Chem. Mater.* **2018**, *30*, 4667−4674.

(5) Abellán, G.; Neiss, C.; Lloret, V.; Wild, S.; Chacln-Torres, J. C.; Werbach, K.; Fedi, F.; Shiozawa, H.; Görling, A.; Peterlik, H.; Pichler, T.; Hauke, F.; Hirsch, A. Exploring the Formation of Black Phosphorus Intercalation Compounds with Alkali Metals. *Angew. Chem., Int. Ed.* **2017**, *56*, 15267−15273.

(6) Korolkov, V. V.; Timokhin, I. G.; Haubrichs, R.; Smith, E. F.; Yang, L.; Yang, S.; Champness, N. R.; Schröder, M.; Beton, P. H. Supramolecular Networks Stabilise and Functionalise Black Phosphorus. *Nat. Commun.* **2017**, *8*, No. 1385.

(7) Kuriakose, S.; Ahmed, T.; Balendhran, S.; Bansal, V.; Sriram, S.; Bhaskaran, M.; Walia, S. Black Phosphorus: Ambient Degradation and Strategies for Protection. *2D Mater.* **2018**, *5*, No. 032001.

(8) Zhu, M.; Kim, S.; Mao, L.; Fujitsuka, M.; Zhang, J.; Wang, X.; Majima, T. Metal-Free Photocatalyst for H_2 Evolution in Visible to Near-Infrared Region: Black Phosphorus/Graphitic Carbon Nitride. *J. Am. Chem. Soc.* **2017**, *139*, 13234−13242.

(9) Zhu, M.; Sun, Z.; Fujitsuka, M.; Majima, T. Z-Scheme Photocatalytic Water Splitting on a 2D Heterostructure of Black Phosphorus/Bismuth Vanadate Using Visible Light. *Angew. Chem., Int. Ed.* **2018**, *57*, 2160−2164.

(10) Lei, W.; Zhang, T.; Liu, P.; Rodriguez, J. A.; Liu, G.; Liu, M. Bandgap and Local Field-Dependent Photoactivity of Ag/Black Phosphorus Nanohybrid. *ACS Catal.* **2016**, *6*, 8009−8020.

(11) Yuan, Y.-J.; Yang, S.; Wang, P.; Yang, Y.; Li, Z.; Chen, D.; Yu, Z.-T.; Zoub, Z.-G. Bandgap-Tunable Black Phosphorus Quantum Dots: Visible-Light-Active Photocatalysts. *Chem. Commun.* **2018**, *54*, 960−963.

(12) Wu, Q.; Liang, M.; Zhang, S.; Liu, X.; Wang, F. Development of functional black phosphorus nanosheets with remarkable catalytic and antibacterial performance. *Nanoscale* **2018**, *10*, 10428−10435.

(13) Shi, F.; Geng, Z.; Huang, K.; Liang, Q.; Zhang, Y.; Sun, Y.; Cao, J.; Feng, S. Cobalt Nanoparticles/Black Phosphorus Nanosheets: An Efficient Catalyst for Electrochemical Oxygen Evolution. *Adv. Sci.* **2018**, *5*, No. 1800575.

(14) Caporali, M.; Serrano-Ruiz, M.; Telesio, F.; Heun, S.; Nicotra, G.; Spinella, C.; Peruzzini, M. Decoration of Exfoliated Black Phosphorus with Nickel Nanoparticles and its Application in Catalysis. *Chem. Commun.* **2017**, *53*, 10946−10949.

(15) Bai, L.; Wang, X.; Tang, S.; Kang, Y.; Wang, J.; Yu, Y.; Zhou, Z.-K.; Ma, C.; Zhang, X.; Jiang, J.; Chu, P. K.; Yu, X.-F. Black Phosphorus/Platinum Heterostructure: A Highly Efficient Photocatalyst for Solar-Driven Chemical Reactions. *Adv. Mater.* **2018**, *30*, No. 1803641.

DOI: 10.1021/acs.chemmater.9b00851
Chem. Mater. 2019, 31, 5075−5080

(16) Wu, T.; Fan, J.; Li, Q.; Shi, P.; Xu, Q.; Min, Y. Palladium Nanoparticles Anchored on Anatase Titanium Dioxide-Black Phosphorus Hybrids with Heterointerfaces: Highly Electroactive and Durable Catalysts for Ethanol Electrooxidation. *Adv. Energy Mater.* **2018**, *8*, No. 1701799.
(17) Köpf, M.; Eckstein, N.; Pfister, D.; Grotz, C.; Krüger, I.; Greiwe, M.; Hansen, T.; Kohlmann, H.; Nilges, T. Access and in Situ Growth of Phosphorene-Precursor Black Phosphorus. *J. Cryst. Growth* **2014**, *405*, 6−10.
(18) Serrano-Ruiz, M.; Caporali, M.; Ienco, A.; Piazza, V.; Heun, S.; Peruzzini, M. The Role of Water in the Preparation and Stabilization of High-Quality Phosphorene Flakes. *Adv. Mater. Interfaces* **2016**, *3*, No. 1500441.
(19) Ribeiro, H. B.; Pimenta, M. A.; de Matos, C. J. S. Raman Spectroscopy in Black Phosphorus. *J. Raman Spectrosc.* **2018**, *49*, 76−90.
(20) Nicotra, G.; Politano, A.; Mio, A. M.; Deretzis, I.; Hu, J.; Mao, Z. Q.; Wei, J.; La Magna, A.; Spinella, C. Absorption Edges of Black Phosphorus: A Comparative Analysis. *Phys. Status Solidi B* **2016**, *253*, 2509−2514.
(21) Militello, M. C.; Simko, S. J. Elemental Palladium by XPS. *Surf. Sci. Spectra* **1994**, *3*, 387.
(22) Militello, M. C.; Simko, S. J. Palladium Oxide by XPS. *Surf. Sci. Spectra* **1994**, *3*, 395.
(23) Caporali, M.; Guerriero, A.; Ienco, A.; Caporali, S.; Peruzzini, M.; Gonsalvi, L. Water-Soluble, 1,3,5-Triaza-7-phosphaadamantane-Stabilized Palladium Nanoparticles and their Application in Biphasic Catalytic Hydrogenations at Room Temperature. *ChemCatChem* **2013**, *5*, 2517−2526.
(24) Kuntz, K. L.; Wells, R. A.; Hu, J.; Yang, T.; Dong, B.; Guo, H.; Woomer, A. H.; Druffel, D. L.; Alabanza, A.; Tomanek, D.; Warren, S. C. Control of Surface and Edge Oxidation on Phosphorene. *ACS Appl. Mater. Interfaces* **2017**, *9*, 9126−9135.
(25) Wang, J.; Liu, D.; Huang, H.; Yang, N.; Yu, B.; Wen, M.; Wang, X.; Chu, P. K.; Yu, X.-F. In-Plane Black Phosphorus/Dicobalt Phosphide Heterostructure for Efficient Electrocatalysis. *Angew. Chem., Int. Ed.* **2018**, *57*, 2600−2604.
(26) Carenco, S.; Hu, Y.; Florea, I.; Ersen, O.; Boissière, C.; Sanchez, C.; Mezailles, N. Structural Transitions at the Nanoscale: the Example of Palladium Phosphides Synthesized from White Phosphorus. *Dalton Trans.* **2013**, *42*, 12667−12674.
(27) Miller, H. A.; Lavacchi, A.; Vizza, F.; Marelli, M.; Di Benedetto, F.; D'Acapito, F.; Paska, Y.; Page, M.; Dekel, D. R. A Pd/C-CeO2 Anode Catalyst for High-Performance Platinum-Free Anion Exchange Membrane Fuel Cells. *Angew. Chem., Int. Ed.* **2016**, *55*, 6004−6007.
(28) Zachariasen, W. H. The Crystal Structure of Palladium Diphosphide. *Acta Crystallogr.* **1963**, *16*, 1253.
(29) Rundqvist, S. Phosphides of the Platinum Metals. *Nature* **1960**, *185*, 31.
(30) Darensbourg, D. J.; Decuir, T. J.; Stafford, N. W.; Robertson, J. B.; Draper, J. D.; Reibenspies, J. H.; Kathó, A.; Joó, F. Water-Soluble Organometallic Compounds. Synthesis, Spectral Properties, and Crystal Structures of Complexes of 1,3,5-Triaza-7-phosphaadamantane with Group 10 Metals. *Inorg. Chem.* **1997**, *36*, 4218−4226.
(31) Blaser, H.-U.; Steiner, H.; Studer, M. Selective Hydrogenation of Functionalized Nitroarenes: An Update. *ChemCatChem* **2009**, *1*, 210−221.
(32) Costantino, F.; Nocchetti, M.; Bastianini, M.; Lavacchi, A.; Caporali, M.; Liguori, F. Robust Zirconium Phosphate−Phosphonate Nanosheets Containing Palladium Nanoparticles as Efficient Catalyst for Alkynes and Nitroarenes Hydrogenation Reactions. *ACS Appl. Nano Mater.* **2018**, *1*, 1750−1757.
(33) Kou, L.; Frauenheim, T.; Chen, C. Phosphorene as a Superior Gas Sensor: Selective Adsorption and Distinct I−V Response. *J. Phys. Chem. Lett.* **2014**, *5*, 2675−2681.

DOI: 10.1021/acs.chemmater.9b00851
Chem. Mater. 2019, 31, 5075−5080